ACS Catalysis

Research Article

pubs.acs.org/acscatalysis

In Silico Screening of Iron-Oxo Catalysts for CH Bond Cleavage

Prokopis C. Andrikopoulos,[†] Carine Michel,[†] Sandra Chouzier,[‡] and Philippe Sautet*[,†]

[†]University of Lyon, CNRS, Laboratoire de Chimie, UMR5182, ENS de Lyon, 69364 Lyon, France

[‡]Research and Innovation Centre Lyon, Solvay Polyamide and Intermediates, 69192 Saint-Fons, France

Supporting Information

ABSTRACT: Inspired by oxidation enzymes such as P450 and TauD, several groups have based their research on the iron−oxo moiety in the field of alkanes partial oxidation. Still, the controlled cleavage and oxidation of the aliphatic C−H bond remains a prized goal in chemistry. We present here a computational methodology to predict the comparative reactivity of iron−oxo complexes for this process from linear relations based on the sole electronic structure of the reactant state. The efficient correlation of the C−H activation barrier to a simple but intuitive molecular orbital descriptor enables the design of ligands that permit low barrier C−H abstraction steps and the fast screening of novel potential complexes. The activation of the catalyst by a multidentate effect is also evidenced. We anticipate this study to improve the rational design of hydrocarbon oxidation catalysts.

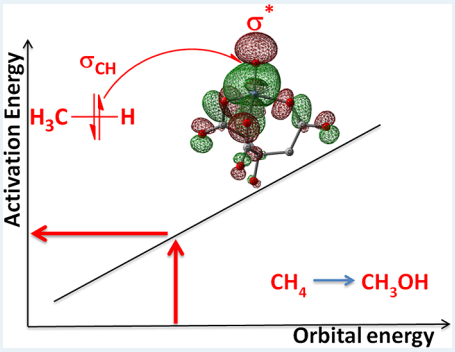

KEYWORDS: *alkane partial oxidation, methane, iron-oxo complex, activation energy, molecular orbital descriptor*

INTRODUCTION

Iron complexes are gradually moving to the forefront of the field of alkane activation.[1−5] These have been inspired by analogue processes in biological systems,[6] where Fe^{IV}=O active sites are responsible for the activity such as the cytochrome-P450 compound-I[7] or the intermediate J of taurine dioxygenase (TauD).[8] In order for iron complexes to cross over to useful applications in industry, an effort in documenting and predicting their properties in a consistent manner has to be implemented—a task that is undertaken here by theoretical means.

The high spin Fe^{IV}=O intermediate is a strong electrophile that can abstract a hydrogen atom from an alkane. A rebound step follows, that forms the C−O bond and leads to the corresponding alcohol.[9] Certain patterns have emerged from the number of iron−oxo complexes that have been recently examined. The C−H abstraction step is expected to be crucial in the full oxidation cycle, the overall kinetics being correlated to the strength of the C−H bond of various substrates.[10] The pK_a of the Fe^{IV}−OH intermediate is also essential to the overall activity as demonstrated recently in cytochrome P450.[11] In other words, the driving force for the C−H activation by the Fe^{IV}=O moiety is given by the difference between the energy of the C−H bond to be broken (BDE_{CH}) and the energy of the O−H bond to be formed (BDE_{OH}). De Visser has rationalized those trends on a family of seven Fe-oxo complexes using DFT calculations: the height of the hydrogen abstraction barrier of propene is linearly correlated to the reaction energy, $\Delta H = BDE_{CH} - BDE_{OH}$.[12] This approach has been generalized recently in a meta-analysis of 13 computational studies on hydrogen abstraction by iron and manganese oxo complexes demonstrating the importance of the reaction driving force.[13] This correlation between the barrier height and the reaction energy is known as the Bell−Evans−Polanyi principle.[14]

Since the pioneering works of K. Fukui[15] and R. Hoffmann,[16] the importance of the interactions between the molecular orbitals of the reagents, and mainly between the frontier orbitals, is well-known as a key parameter governing reactivity. In the CH abstraction step, the proton transfer to the oxo-oxygen is coupled to an electron transfer from the σ(CH) of the alkane substrate to the lowest vacant acceptor orbital of the electrophilic Fe^{IV}=O group.[17,18] The qualitative role of several parameters was underlined for this interaction from the electronic structure calculations of octahedral Fe^{IV}=O complexes.[19−23] Shaik and co-workers stressed the influence of the overlap between the alkane σ(CH) and the acceptor orbitals on the complex to determine the structure of the transition state. Baerends and co-workers noted the crucial importance of the energy of the acceptor orbital. On a set of four model complexes with water as equatorial ligands, they were able to modulate the energy of the acceptor orbital by the nature of the axial ligand and modify the calculated barriers. However, to the best of our knowledge, those qualitative analyses were not transformed into a detailed and predictive correlation between the C−H abstraction barrier and a well-defined electronic structure parameter of the initial complex. Such a correlation would supplement the existing ones derived from the BEP principle providing a fundamental and easy descriptor of the Fe^{IV}=O activity.

Received: July 12, 2014
Revised: March 10, 2015
Published: March 10, 2015

DOI: 10.1021/cs500996k
ACS Catal. 2015, 5, 2490−2499

The possible spin states of d^4 Fe^{IV}=O intermediates are S = 0, 1, or 2 depending on the ligand field. The singlet state (S = 0) is generally very unstable and will not be considered here, the ground state of the complexes being either the triplet (S = 1, called here low spin (LS) for simplicity) or quintet state (S = 2, called here high spin (HS)). In the presence of strong enough donor ligands, (typically nitrogen based), octahedral Fe^{IV}=O intermediates have a triplet low spin (LS) state, the lowest acceptor orbital being generally the so-called β–π^* (antibonding combination of d_{xz}(Fe)/d_{yz}(Fe) and p_x(O)/p_y(O) in the β manifold; see Figure 1a). The corresponding

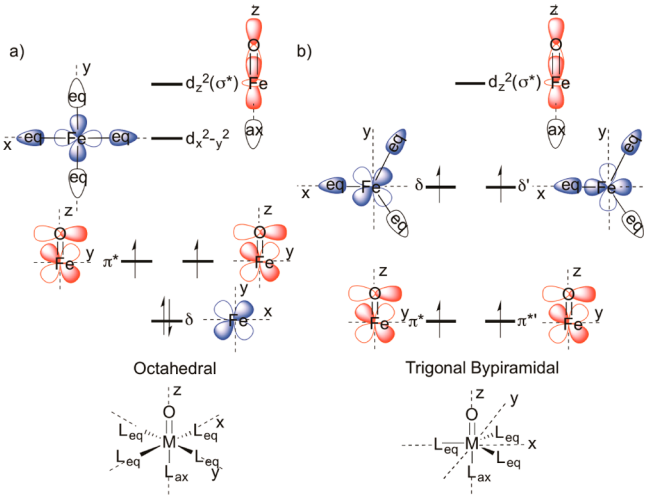

Figure 1. Frontier molecular orbitals of (a) an octahedral Fe-oxo complex in a low spin configuration including the interaction with the equatorial (in the x, y plane) and axial (along the z axis) ligands. In the high spin configuration, the down-spin electron from the δ orbital is promoted to the $d_{x^2-y^2}$ orbital, resulting to a total of four unpaired electrons and (b) a trigonal bipyramidal Fe–oxo complex in a high spin configuration. In this simplified representation up and down spin orbitals are shown with the same energy.

reaction channel is the LS-π path. The proton transfer is coupled to the electron transfer from the σ(CH) of the alkane to the π^*(Fe^{IV}=O). This electronic interaction requires a perpendicular orientation between the CH bond and the Fe^{IV}=O bond, leading to a bended transition state.[24] In the HS state, two types of possible acceptor orbitals are competing, defining two reaction channels: the β–π^* and the so-called α–σ^* (antibonding combination of d_{z^2}(Fe) and p_z(O) in the α spin manifold of molecular orbitals).[25] The β–π^* opens a HS-π path, similar to the LS-π path. The α–σ^* orbital is generally the lowest acceptor orbital on the Fe^{IV}=O fragment due to the considerable electron exchange stabilization of the α molecular orbitals manifold in the S = 2 configuration.[26] This α–σ^* acceptor orbital opens a HS-σ path, where the electronic interactions lead to a linear transition state, the CH and the Fe=O bonds being collinear. This alignment favors the frontier orbital overlap[27] and reduces the Pauli repulsion between the alkane and the ligands.[23] These reaction channels have been described in more details in recent reviews.[18,28,29] Later in the text, the α–σ^* will be noted simply as σ^* and the β–π^*, simply as π^*.

This active HS-σ path can be reached by weakening the ligand field and a common strategy is to reduce the number of donor ligands in the equatorial plane. One approach is to create a trigonal bipyramidal configuration at the iron with the oxo-oxygen along the axis of the pyramid and three nitrogen type ligands in the equatorial plane, while one N atom holds the other axial position.[30,31] This configuration ensures a high spin ground state (Figure 1b) that is preserved along the hydrogen abstraction step. Another strategy to reach the most active state is the spin crossover from a low spin (S = 1) ground state to a high spin (S = 2) excited state in a two-state reactivity mechanism popularized by Schröder, Shaik, and Schwarz.[32] An indication of its energetic cost is provided by the HS–LS adiabatic gap. The lowest energy path for the reaction is then determined by a comparison of the barrier of the LS-π path against the sum of the HS-σ path barrier and the spin gap.

The working hypothesis of the present paper asserts that the C–H abstraction barrier and the lowest acceptor orbital energy of the initial Fe=O complex are correlated: the lower the acceptor orbital energy, the lower the energy barrier would be. For a high spin ground state complex, the barrier will be related to the energy of the σ^* acceptor orbital (HS-σ path). For a low spin ground state, the barrier will be related to the energy of the π^* orbital (LS-π path). In this latter case, the high spin S = 2 excited state will also be considered. Its σ^* energy will be related to the corresponding HS barrier to compare the multistate reactivity with the LS-π path. These basic qualitative effects were outlined in the original works by Baerends[19−21,27,33] and Shaik.[18,26,32] The work presented here will demonstrate how these can be expanded into a valuable tool for catalyst prediction employing an extensive set combining model and realistic catalysts to establish a correlation between the activation energy and the energy of the lowest acceptor orbital (σ^* for the HS path and π^* for the LS path).

RESULTS

In order to test this hypothesis and demonstrate the correlation, a large data set of iron-oxo complexes was chosen, shown in Figures 2 and 3 (see also the *XYZ* coordinates in the Supporting Information (SI)). The choice of systems was made from popular ligands from the literature,[5] porphyrin complexes,[3] iron ligands from chemical databases, and simple model systems, while methane was the chosen substrate. Since the focus of the paper is on the influence of the ligand, the substrate was not changed. A conscious effort was made to obtain a diverse set of ligands that span the whole range of lowest acceptor orbital energies. The first set, shown in Figure 2, is comprised of complexes with a total charge of 2+. This set mixes model complexes designed to rationalize trends (**1**–**12**, **23**–**28**) and also complexes selected from the literature (**13**–**22**, **19**–**38**)[5] to provide a direct comparison with experiments. This set includes a variety of complexes with mainly N donors: cyclams (TMC **34**–**36**),[34,35] bicyclic bispidine ligands (**32**, **33**),[36] tripodal ligands motifs with pyridyl (TPA **17**), guanidine (TMG3tren **18**), amino (Me6-TREN **22**), or benzimidazole (Me3NTB **37**) groups,[37,38] EDTA (**38**), etc. Those complexes are included, as is customary, without the counterions that would balance the total charge and in some cases, complete the metal coordination.[30]

The second set (Figure 3) covers neutral complexes, selected from the literature[5] or derived from commercially available ligands and Fe complexes. Complexes belonging to the first group can be shifted to the second group by including the omitted counterions. The influence of those counterions can be quite complex[39] and will not be covered extensively in this study. The division in two sets is required since the energy range of the acceptor orbitals differs according to the charge

DOI: 10.1021/cs500996k
ACS Catal. 2015, 5, 2490–2499

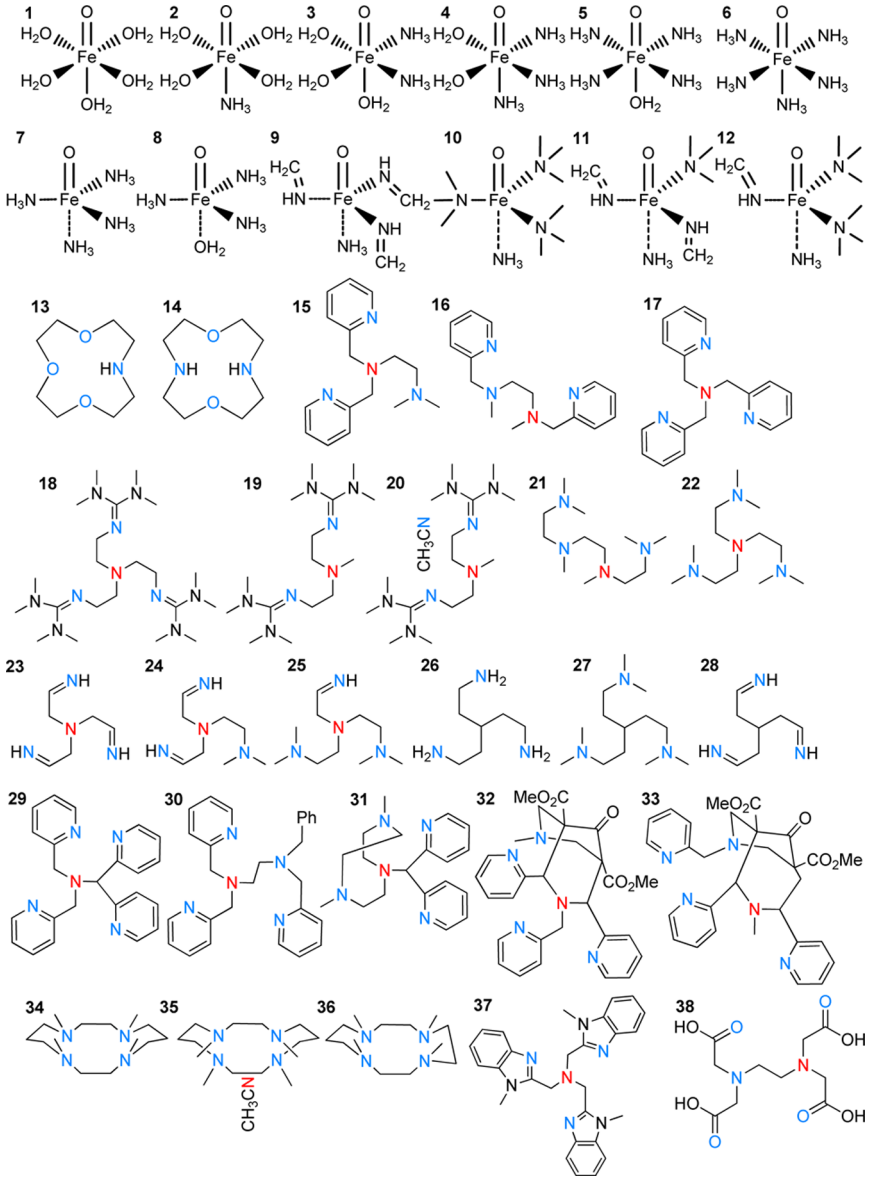

Figure 2. Structure of the complexes with an overall positive charge of 2 included in the first correlation plot. **1**−**12** is the subset of complexes with monodentate ligands, and the drawing includes the position of the Fe═O moiety. **13**−**38** is the subset of polydentate ligands. The position of the Fe═O group is not included for clarity. Atoms coordinated to Fe in the equatorial position are shown in blue, while those in the axial position are in red.

(−14 to −8 eV and −6 to −2 eV for 2+ charged and neutral complexes, respectively). Other popular ligands could be incorporated, such as the negatively charged pyrrolide or urea ones,[40,41] provided an extensive complex set is constructed for their respective charge group, similarly to the 2+ and neutral sets presented here.

The "reactant complex" state, where methane is loosely oriented toward the oxo oxygen (typically 2−3 Å apart) and the transition state structures were then determined to compute the activation barriers E^{ACT}(LS-π path) and E^{ACT}(HS-σ path). In order to accurately compare HS-σ and LS-π paths, reliable predicted spin gaps are required (E^{GAP}). The chosen combination of OPTX (exchange) and PBEc (correlation) functionals with the Dunning's correlation consistent basis sets employed here is known to perform well in this respect.[42] For example, in comparison to CCSD(T) calculations performed by Shaik and co-workers on penta-ammoniated iron oxo (complex **6** here),[43] the quintet-triplet spin gap is estimated accurately (1.3 kcal·mol^{-1}) while the LS-π and HS-σ barriers are not as underestimated as with the popular hybrid B3LYP functional.

A clear correlation was obtained for the first group (**1**−**38**, charge 2+) for the HS-σ path between the activation energy for CH bond dissociation on the HS oxo complexes and the energy of the lowest acceptor σ^*(Fe═O) orbital (HS-σ path, black and blue symbols in Figure 4). Crosses and diamonds signify whether the HS-σ path is associated with a ground or excited state of the initial complex, respectively. From the presence of the 2+ charge, the energy of the σ^*(Fe═O) orbital can be quite low, lower than the HOMO energy of methane in gas phase. However, the HOMO of methane is markedly stabilized in the reactant complex, where it is in the field of the dication, and its energy is again below that of the σ^* acceptor orbital. Evidently, the correlation can be directly applied in order to

DOI: 10.1021/cs500996k
ACS Catal. 2015, 5, 2490−2499

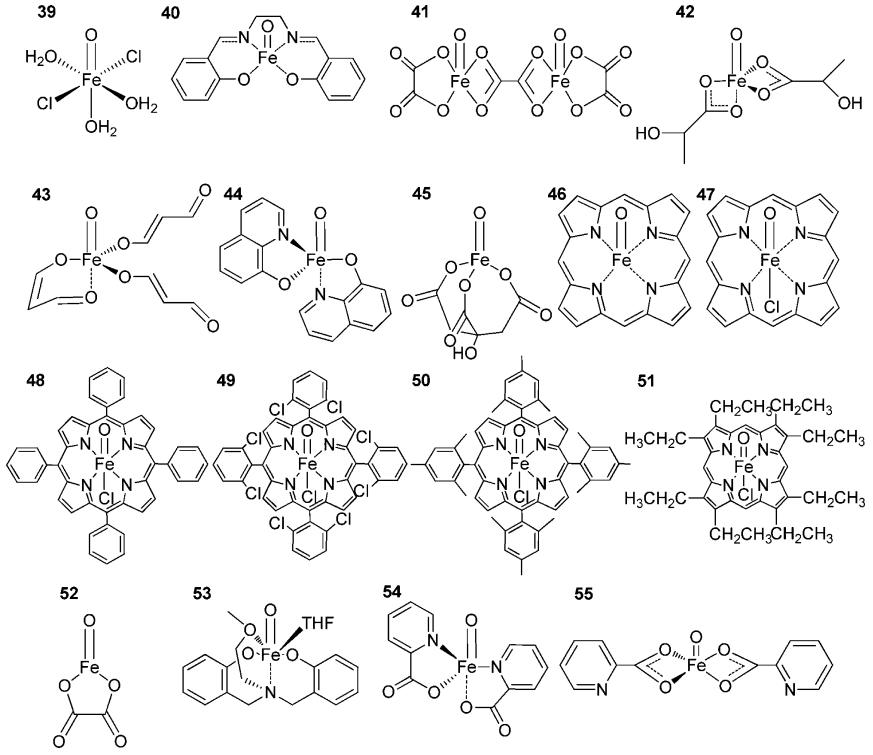

Figure 3. Neutral complexes included in the second correlation plot. All drawings here include the approximate position of the Fe=O moiety.

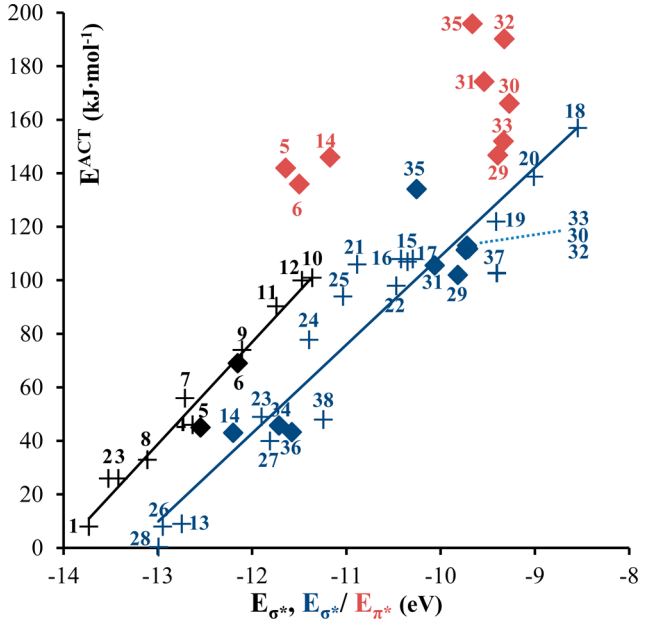

Figure 4. Correlation between the energy of the σ^* orbital of the Fe−oxo complex in electronvolts (x-axis) and the barrier height of the C−H abstraction step in kilojoules per mole (y-axis) for models **1**−**38** (HS-σ path). Two subsets are distinguished: (**1**−**12**) in black and (**13**−**38**) in blue. Crosses indicate complexes with a high spin ground state (quintet), while diamonds indicate those with a low spin (triplet). In addition, for the Fe=O complexes with a LS ground state, the activation energy for C−H abstraction along the LS-π path is also plotted as a function of the energy of the π^* orbital (red diamonds) even if in this case no correlation appears.

obtain the total barrier when dealing with HS ground states, which constitute the majority on this set, or combined with the LS-HS gap, (ideally, with a calculated minimum energy crossing point (MECP)), when dealing with LS ground states. Two subsets of linear relations clearly emerge, and they correspond to different types of ligands.

The first subset (black, **1**−**12**) shows an R^2 value of 0.97, a slope of 38, and a mean absolute deviation (MAD) of 4 kJ·mol^{-1}. In this set, all ligands are monodentate. Models **13**−**38** in Figure 4 (blue) form the second trend-line which is almost parallel to the previous one with a slope of 33, an R^2 value of 0.90, and an MAD of 11 kJ·mol^{-1}. All ligands are here polydentate with three to six coordination sites. In particular, **15**−**18**, **20**−**25**, and **37** are forming with the Fe=O moiety a complex of trigonal bipyramidal geometry.

Overall, the two trend lines reveal a close-fitting linear relation between the energy of the acceptor σ^* orbital and the activation energy. The activation energy of the LS-π path points are also included as a function of the energy of the π^* for the low spin ground state complexes **5**, **6**, **14**, and **29**−**36** (red diamonds). A meaningful correlation cannot be obtained here between the activation energy on the LS-π path and the π^* acceptor orbital energy. The typical bended transition state probably induces a larger variation in the steric hindrance contribution to the activation barrier. For instance, in the TMC−CH_3CN (**35**) complex, the cyclam scaffold hinders the methane approach, leading to a FeOH angle 132° while in the N4Py (**29**), the FeOH angle is smaller (121°), indicating a lower steric hindrance. Despite a similar π^* energy, their activation energy differs by 49 kJ·mol^{-1}.

For the second group of neutral complexes (**39**−**55**), a correlation of the same nature is obtained for the HS-σ path, shown in Figure 5 with black symbols and line. The complexes in this set are less uniform than those of the previous group and show a narrower orbital energy range than for the **1**−**38** group (~3 eV).

The heme Fe−oxo complexes with a Cl axial ligand included here (models **47**−**51**) that originate from a Fe^{III} bare site

DOI: 10.1021/cs500996k
ACS Catal. 2015, 5, 2490−2499

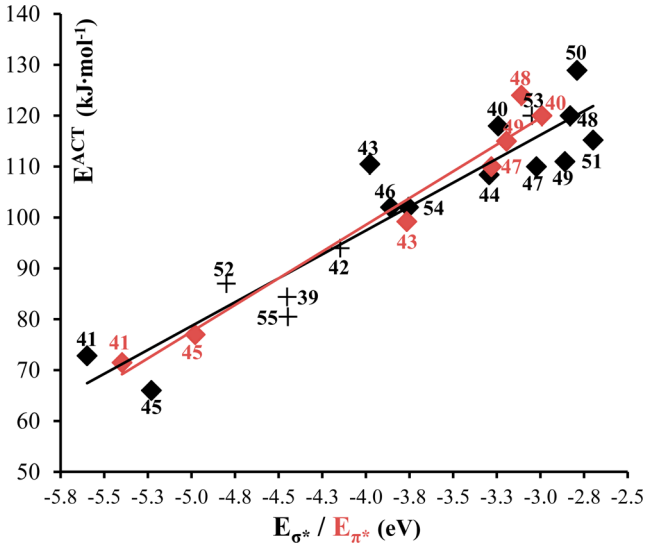

Figure 5. Correlation between the energy of the σ^* orbital of the Fe−oxo complex in electronvolts (x-axis) and the barrier height of the C−H abstraction step in kilojoules per mole (y-axis) for models **39**−**55**, shown in black with all complexes considered in the high spin state (HS-σ path). Crosses indicate complexes with a high spin ground state (sextet/quintet), while diamonds those with a low spin (quartet/triplet). The correlation between the barrier height of the C−H abstraction step (on the low spin surface) and the energy of the π^* of certain low spin ground state models is also included with red diamonds and line (LS-π path).

display the typical ligand radical configuration O=Fe^{IV}($Por^{\bullet+}$)-(Cl^-) and hence correspond to a quartet ground state (called low spin here) and a sextet high spin excited state. Remarkably, the nonheme complexes **43** and **45** that also originate from a Fe^{III} bare site attain a similar configuration O=Fe^{IV}($L^{\bullet+}$). While in heme containing systems the LUMO is typically located mainly on the heme, and in **43**−**45** it is located on the ligand, the C−H abstraction will be initiated normally through the acceptor orbital Fe^{IV}=O(π^*) or Fe^{IV}=O(σ^*).[26] This allows heme containing systems to be included in the correlation.The transition state structures of this neutral group display Fe−O−H angles much lower than 150° (see SI Table S2) typical of a π-path motif. However, the orbital analysis of those transition state structures reveals that the forming bonding orbitals are of substantial σ^* character (e.g., 35% σ^* for the HOMO the transition state structure of **46** with a Fe−O−H angle of 137.5°) which explains their correlation preference with the σ^* energy levels.

No distinct monodentate/polydentate lines are established in this correlation since only one model is exclusively monodentate (**39**). Despite the high heterogeneity of the set, the quality of the correlation is also of high standard with an R^2 value of 0.87 and an MAD of 5 kJ·mol^{-1}.

For several of the low spin ground state models, the relation between the energy of their respective π^* orbital and the activation energy along the low spin PES (LS-π path) is also included in the neutral correlation plot (Figure 5, red). In contrast with the case of the charge 2+ complexes, a good correlation is also obtained here. As mentioned before, to predict the minimum energy pathway, one would only have to compute the spin gap between the two spin variants and then compare the activation barriers obtained from the linear relation on the two spin PESs, simply from the calculation of the energies of the HS state σ^* orbital and the LS state π^* orbital. In the case of the LS path, although most of the complexes show large activation energy in the right part of Figure 5, some of them counterintuitively yield a small barrier (**41**, **45**, and even **43**). This shows that, if the π^* orbital is low enough, the LS-π pathway in the case of neutral systems can also provide efficient systems for CH activation (we again stress that by LS we mean quartet/triplet cases).

The correlations in Figures 4 and 5 illustrate that not only high spin ground state complexes (shown as crosses) can be expected to lie along the linear relation but also high spin excited states (shown as diamonds), isomers, regardless of their relative stability (**54** and **55**), bimetallic complexes (**41**), heme-containing systems, inferring that iron-oxo orbitals facilitate the electron transfer to the porphyrin ring (**46**−**51**), and, as mentioned before, complexes with radical ligands (**43**, **45**, **47**−**51**; see Tables S1, S2, and S3 in the SI for details).

DISCUSSION

These correlations provide, on both sets of ligands, a fast prediction of the H-abstraction activation energy E^{ACT}(HS-σ path) on the S = 2 potential energy surface and in the case of the neutral molecules also for E^{ACT}(LS-π path) on the S = 1 potential energy surface. The MAD for the activation energy ranges between 4 and 11 kJ·mol^{-1}, which is reasonably low for a first screening of a large potential set of ligands, provided that they correspond to the same charge for the (L)Fe^{IV}=O complex. This translates into a deviation of ∼0.3 eV for the characteristic orbital energy (σ^* or π^*) of the Fe−oxo complex, and hence the approach cannot discriminate cases where acceptor orbital energies are too close.

For the +2 charge complexes, the correlation provides the C−H activation barrier in the quintet (HS) spin manifold, but this is the overall barrier only if the reactant complex is a spin quintet. For triplet complexes (diamonds in Figure 4), the spin gap should be added, since spin−orbit coupling should yield a high probability for spin inversion and open the two state reactivity mechanism.[32] The correlation provides the activity order between two complexes only if the change in HS barriers dominates the variations in spin-gap. In the opposite case where the spin-gap variation dominates, reactivity prediction is out of reach of our correlations.

The division of the charge 2+ catalysts in two correlation subsets (monodentate/multidentate) is remarkable and was not underlined before. It shows that the energy of the σ^* orbital is not the only criterion governing the CH dissociation energy. For a given value of the σ^* energy, the presence of the multidentate scaffold tends to lower the activation energy by ∼25 kJ·mol^{-1}. In the case of independent monodentate ligands, Fe is close to the plane of the equatorial ligands, in a rather perfect geometry. This is not the case for the multidentate ligands where the constraint imposed by the scaffold prevents the coordinating atoms to occupy their optimal position in the equatorial plane (see the SI). As a result the Fe and equatorial ligand show a pyramid shape, the ligands being bent away from the oxo group, and this distortion is often stronger in the TS than in the reactant state (see Table S1, S2, and S3 in the SI). In other words, the Fe^{IV}=O unit is pulled out above this plane (see also SI Figure S2). The correlations presented stem from the dominating two electron interaction between the C−H occupied orbital and the Fe-oxo acceptor orbital. The four-electron interaction between occupied states on methane and on the ligands is however non-negligible. Upon its approach,

DOI: 10.1021/cs500996k
ACS Catal. 2015, 5, 2490−2499

methane feels less Pauli repulsion from the pyramidal Fe=O with multidentate ligands than from complexes with monodentate ligands and this leads to a more favorable transition state energy at a given σ^* energy. This effect will depend on the multidentate ligand which gives more scatter in the multidentate line (**13**−**38**) than in the case of the model complexes (**1**−**12**). The use of a multidentate ligand is also known to increase the catalyst stability by reduction of the ligand lability. Thus, using a multidentate scaffold is essential to improve the design of Fe^{IV}=O catalysts as it provides gains in stability *and* activity at once.

These correlations have been established with the OPBE exchange correlation functional and in the gas phase. It is important to assess their general character. For practical reasons this has been performed on the subset of complexes **1**−**12** and on the HS surface. A second functional has been tested, B3LYP-D, and it also provides a clear linear relation. However, if the existence of a correlation between acceptor orbital energy and activation energy is general, the slope and offset are dependent on the chosen functional (see SI Figure S4). The second method-related question concerns the influence of solvent. The implicit PCM method has been considered for three different solvents (cyclohexane, acetonitrile, and water), and the resulting activation energy/acceptor orbital energy relations are shown in Figure 6. A linear relation of high quality

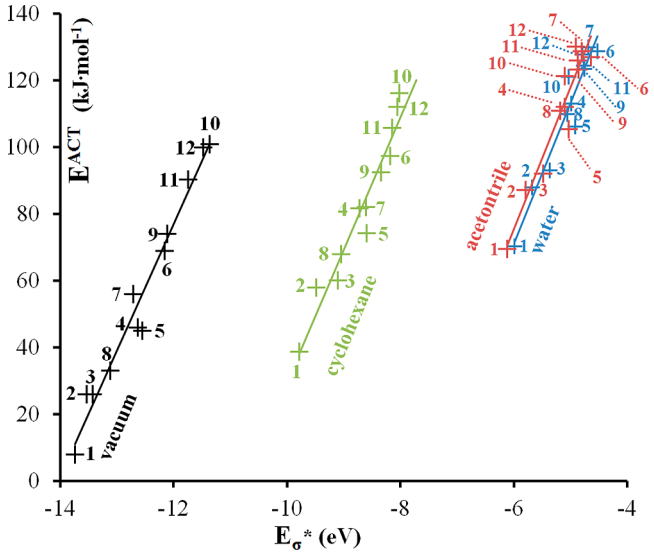

Figure 6. Correlation between the energy of the σ^* orbital of the reactant in electronvolts (x-axis) and the barrier height of the C−H abstraction step in kilojoules per mole (y-axis) for models **1**−**12** (HS-σ path), demonstrating the solvation effect. Green crosses and line refer to cyclohexane (ε = 2.02), red to acetonitrile (ε = 35.69), and blue to water (ε = 78.36) implicit solvent calculations. The gas phase calculations are recalled for comparison with black crosses and line.

holds for each choice of solvent. The solvent simply shields the positive charge, so that the σ^* orbital energy is less stabilized, the effect being smaller with cyclohexane with low dielectric constant and saturating for acetonitrile/water. The proposed linear relation hence still holds in the presence of a solvent, and the slope is unchanged within error bars. At the same time, the solvent increases the C−H activation barrier for a given ligand, and the effect is stronger for highly polar solvents. This explains the preference for a low polarity solvent, like the alkane itself, for alkane partial oxidation with Fe−oxo complexes. This effect is however dependent on the choice of ligand, since this choice affects the electrostatic properties of the complex, the barrier for **10** being increased by only 20 kJ·mol^{-1} between vacuum and water, while that of **7** is increased by 77 kJ·mol^{-1}. Hence the reactivity order between various ligands is dependent on the choice of solvent, e.g. **7** is more reactive than **9** and **10** in cycloxexane but less reactive in acetonitrile.

Therefore, once calibrated with a few points, such relations represent a practical way to evaluate the activation barrier on the HS surface, with several exchange correlation functionals and solvent polarities, since it only requires to calculate the energy of the σ^* orbital in the Fe−oxo complex. It has also a strong potential to be extended to other catalytic reactions.

Beyond this numerical aspect, the linear relation also provides simple chemical insight since it allows us to link the CH bond dissociation activation energy for a given spin state with a simple quantity, the energy of the lower lying acceptor orbital of the Fe^{IV}=O catalyst, for which we have many guidelines from molecular orbital theory. The energy of this orbital is simply related with the electronic character of the ligands, electron donating ligands pushing it to higher energy and electron withdrawing ones in contrast lowering its energy, and hence yielding a lower barrier for CH activation. This can give simple and powerful design ideas to the chemists.

This effect is clearly illustrated on the first subgroup of the first set (models **1**−**12**, black line). Weakly donating H_2O ligands are progressively substituted by stronger amine type donors (**1**−**8**), shifting up the σ^*(Fe=O) orbital. From the shape of the d_{z^2}(Fe) orbital, the substitution of the axial ligand is more effective than that of the equatorial ones as already discussed in the literature[44] and nicely illustrated experimentally on a cyclam series.[45]

As indicated in the introduction, a BEP type linear relation has been proposed earlier on a set of Fe and Mn oxo complexes, linking the H abstraction barrier to the reaction energy ΔE.[12,13] In the present paper, the reactivity descriptor is not the total reaction energy, but an electronic structure parameter: the energy of the (initially vacant) acceptor orbital of the Fe−oxo complex. Although both types of relations are potentially interesting, one advantage of the present approach is that as said just above, molecular orbital theory gives us qualitative tools to predict the variation of the σ^* energy as a function of the type of ligands.

These correlations have been established with GGA exchange correlation functionals (OPBE mainly, and B3LYP-D in one case) that have already proven a reasonable accuracy for the electronic structure and catalytic reactivity of coordination complexes. To the best they would reproduce the DFT energy and hence cannot perform better than these for the comparison with experimental results. In addition, the intrinsic error forbids distinguishing ligands that yield similar energy for the acceptor orbital, in a window of 0.3 eV, and cases where the complex is not high spin add the complication of the spin-gap. Some of the mentioned complexes are comprised of model ligands and this type of ligand searches should ideally be performed in tandem with experimental work. Hence, we will now discuss how the results from the linear relations compare with experimental data on the reactivity of iron oxo complexes. Such a comparison should optimally be performed by comparing to measured reaction rates.

The guanidyl ligand series (**18**−**20**) nicely demonstrates how the modulation of the donor properties of the ligand enables to tune the reactivity, in the case of complexes with charge +2 and

DOI: 10.1021/cs500996k
ACS Catal. 2015, 5, 2490−2499

with a HS quintet ground state. From TMG3tren (**18**) to TMG2dien−CH_3CN (**20**), one arm of the ligand is removed and a solvent molecule CH_3CN occupies the vacant equatorial coordination site. The change for a weaker donor ligand pulls down the energy of the σ^* orbital by 0.47 eV and activates the Fe^{IV}═O core. The HS barrier is here the global C−H activation barrier and is reduced by 18 kJ·mol^{-1}, in agreement with the experimental gain in the kinetic constant, by a factor of 630 for 9,10-dihydroanthracene.[37] A further activation can be realized by the removal of CH_3CN solvent molecule (**19**). Again, the σ^* orbital is stabilized (by 0.4 eV) and the activation barrier is reduced by an extra 17 kJ·mol^{-1}.

The reactivity of the Fe-oxo complex with benzimidazol **37** has been evaluated in the same conditions as **18** and **20**, and it was found to be 100 to 3000 times more reactive than **18**.[38] The Fe−oxo complex initially coordinates a solvent CH_3CN and is low spin (S = 1), but it is likely that the solvent molecule departs to form the reactive trigonal bipyramidal high spin (S = 2) complex. Compared to **18**, **37** reduces the donor capacity of the equatorial N groups, which move the σ^* orbital 0.9 eV to lower energy. As a result the barrier on the HS surface is markedly reduced, in relation with the experimental result.

The cyclam family (**34**−**36**) remains on the charge 2+ case but shows a LS triplet ground state. The contraction of the scaffold with one carbon less in TMC-13 (**36**) than in TMC-14 (**34**) has little influence on the energy of the σ^* orbital, nor on the spin-gap (see SI Table S1). Experiment however shows that, if acetonitrile is used as solvent, the iron−oxo complex with **34** accepts a solvent molecule in axial position (noted **35**).[46] The strong effect of a donor ligand in axial discussed above pushes the σ^* orbital to higher energy by 1.5 eV and hence, following the linear relation, strongly increases the C−H dissociation barrier on the HS surface. In principle the spin-gap from triplet to quintet in the reactant complex should be added to obtain the global barrier, but the effect is large enough (90 kJ·mol^{-1}) here to allow a direct conclusion. The contracted ring of **36** is too narrow to allow the coordination of acetonitrile and the axial position remains vacant, hence keeping a low σ^* orbital and a high reactivity. This is in good agreement with experiment where the complex TMC-13 (**36**) is much more reactive than that with TMC-14 (**34**) in acetonitrile. From our linear relations one can suggest a further modification in the cyclam family **34**−**36**. In addition to the ring contraction to remove the acetonitrile, one can also play on the nature of the donor atom, replacing nitrogen by oxygen hence leading to aza-crown ether (**13**, **14**).

The comparison of the reactivity of a low spin and a high spin complex should be done with care. **20** and **29** have been experimentally studied in similar conditions, and **20** is 15−30 times more active than **29**, depending on the substrate. Figure 4 indicates that **20** presents a σ^* orbital 0.8 eV higher in energy and, following the linear relation, a barrier of 139 kJ·mol^{-1} on the HS surface, 37 kJ·mol^{-1} larger than that of **29**. This could seem in disagreement with the experiment, but disregards the fact that **29** is a low spin complex. The barrier on the LS surface is calculated at 147 kJ·mol^{-1}, and the promotion from the LS to the HS state for the reactant costs 52 kJ·mol^{-1}, which puts the global barrier through the HS TS at 154 kJ·mol^{-1}. Hence **29** is calculated to be less active than **20**, well in line with the measured reactivity.

Recently, the oxidative properties of a series of N5 ligands have been investigated experimentally by varying the N-donor groups (pyridyl, bispidine, or amino, **29**−**33**).[47] Charge 2+ octahedral Fe-oxo complexes are obtained and their ground state is a triplet. The five points fall very close to the linear fit of Figure 4, but the corresponding σ^* energies only differ by a maximum of 0.25 eV (less than the error related uncertainty for the σ^* energies of 0.3 eV) and points **30**, **32**, and **33** almost overlap. The range in calculated activation energies on the HS surface is hence also small (E^{ACT} = 102−113 kJ·mol^{-1}). In addition since the complex are low-spin, the spin gap should be added to the HS activation energy to obtain the global activation energy. In fact, the variation of the triplet-quintet energy gaps is much larger than that of the HS barriers and controls the relative activity (E^{GAP} = 26−52 kJ·mol^{-1}). Hence, we are here clearly at the limit of applicability of the method. For instance, the two bicyclic bispidine (**32**, **33**) have almost the same HS barrier around 110 kJ·mol^{-1}. The observed greater activity of **33** lies in the spin gap, 15 kJ·mol^{-1} smaller than that of **32**. Similarly, **31** is 10 times more active than **29**, while the HS barriers are 106 and 102 kJ·mol^{-1}, respectively. The correct order in barriers is retrieved after addition of the spin gaps to obtain the global barriers, respectively 142 and 154 kJ·mol^{-1}. For this family of low spin complexes, the reactivity is not controlled by the energy of the σ^* orbital (since changes are small) but rather by variations in the spin gaps and possible influence of the second coordination sphere.[48]

The last comparison with experiment will focus on the set of neutral complexes. Synthetic porphyrins were among the first complexes to be involved in the biomimetic C−H oxidation effort.[3] First generation iron porphyrins (Fe^{III}TPPCl, **48**) perform well for various partial oxidation reactions, such as the cyclohexane to cyclohexanol conversion.[49] Our approach (Figure 5) fittingly predicts the superiority of the TPP (tetraphenylporphyrin) and TDCPP (tetrakis (2, 6-dichlorophenyl)porphyrin) (**48** and **49**, respectively) over the TMP (tetramesitylporphyrin) type (**50**).[50−52] The axial ligand effect in porphyrins is known to differ from the nonheme complexes: a stronger donor leads to a greater activity.[53] The induced variations of reactivity have been shown to correlate mainly with the stability of the intermediate and the ease of the rebound step.[49] Those effects are out of reach of our simple screening approach based on the electronic structure of the Fe═O complex.

In final, it is important to underline that comparisons with experiments have to be considered carefully as a relevant article by Nam and co-workers demonstrates,[54] since yields and alcohol to ketone ratios depend profoundly on the respective conditions, such as the type of solvent used, the amount and kind of oxidant, and the manner the various counterions interact with the metal center. Nevertheless, if one keeps in mind the limited accuracy in acceptor orbital energy (0.3 eV) and the fact that these correlations mainly apply to the HS energy surface, the above comparisons validate our approach.

As a consequence, these correlations have a potential for the design of optimal ligands, specifically tuned to minimize the C−H activation energy using Fe−oxo complexes. A strategy to lower the reaction barrier can be, for example, to replace strongly electron donor trimethylamine ligands by imine ligands in the equatorial plane as illustrated on simple model systems (**22** → **24** → **23**). An even more efficient approach is to act on the axial ligand and to replace it by a noncoordinating carbon atom (i.e., **22** → **27**). This switches from a tetradentate to a tridentate ligand and blocks the axial position of the complex, yielding a strong reduction of both the σ^* energy and the CH activation barrier. These two strategies can be

DOI: 10.1021/cs500996k
ACS Catal. 2015, 5, 2490−2499

combined and this leads to an optimal model complex with a predicted barrierless C−H abstraction in vacuum (**28**, E^{ACT}: 0.3 kJ·mol^{-1}) and hence a low barrier in cyclohexane. Hence, from the analysis of the first set of complexes (2+ charge), several guidelines can be extracted to design efficient nonheme oxidation catalysts based on the Fe^{IV}=O moiety. One should try to reach a high-spin Fe^{IV}=O active species with a low lying σ^* orbital combining (i) a weak equatorial ligand field, using in particular a tridentate ligand, and (ii) the weakest possible axial ligand field, blocking the axial site with noncoordinating carbon, for instance.

To propose potential efficient oxidation catalysts, one can also target the neutral oxo complexes of the second set (Figure 3) extracted from literature such as heme-complexes[50−52] or derived from commercially available Fe complexes. Such a choice of neutral complexes avoids spurious effects of counterions. The porphyrin complexes included in this work are found in the right section of the correlation plot (Figure 5, **46**−**51**) with computed barriers for the C−H dissociation step of over 100 kJ·mol^{-1}. The computational screening and the proposed σ^* energy descriptor however underlines much more efficient systems and predicts the complexes found well to the left on the correlation line (e.g., **41**, **42**, **45**, **52**) as prime candidates for the task. Following the strategies extracted from the model systems analysis, they exhibit a weak equatorial ligand field, no ligand in the axial position and a first coordination sphere replete by the multidentate ligand. The high activity of these complexes is a prediction from our study since to our knowledge they have not yet been tested for alkane partial oxidation yet. A potential limitation is that these complexes also correspond often to weak metal ligand interactions (see SI Figures S3a and b) so that their stability might be an issue. They might appear only as short-lived intermediates in the catalytic cycle. However, some possible candidates combine a reasonable stability and good activity. Complex **45** derived from Fe^{III}−citrate, specifically tried because of the resemblance with **26**−**28**, is the most stable of the neutral set by virtue of its strongly donating carboxylate groups. However, it also combines a trigonal equatorial ligand sphere and an axial site being blocked by a noncoordinating carbon in a multidentate ligand. Therefore, its low-spin ground state exhibits a low-lying π^* that opens the LS path with a reasonable activation barrier (E^{ACT} = 77 kJ·mol^{-1}). Interestingly, this path is more active than the two-state scenario (spin crossing and HS-transition state). This potential catalyst demonstrates that design strategies could also target the LS path efficiently using the correlation we have established here. Next, the very simple Fe^{II}−oxalate complex (**52**), provided that no extra strong ligand could coordinate Fe in the reaction media, or the associated dimer (**41**) seem to be other very promising catalysts. The reasonable stability of the Fe^{IV}=O-oxalate is combined with good activity (E^{ACT} = 87 kJ·mol^{-1}), enrooted in an HS ground state and a low-lying σ^*. It would be of great interest to test those candidates experimentally. Then, the potential synthetic modifications of those complexes could be tested primarily in silico using the correlation presented in this article. These potential catalysts have been evaluated in the absence of solvent. Our model study (Figure 6) however indicates that a solvent with low dielectric constant and weak coordinating capabilities, as cyclohexane, is the best choice, while acetonitrile, frequently used in the literature, might not be the optimal solvent due to its ligand capability.

CONCLUSION

Clear linear relations have been demonstrated between the activation energy for C−H dissociation on the HS (sextet/quintet) energy surface and the σ^* acceptor orbital of the initial (L)Fe^{IV}=O complex. In addition for the neutral LS oxo complexes (quartet/triplet) a relation between π^* acceptor orbital and activation energy on the low-spin surface also holds. Although initially established for the OPBE functional, these linear relations have a general character, however the relation parameters (slope and offset) can depend on the choice of functional and on the solvent. Comparison with experiments validate the concept, although these comparisons have to be performed with care due to the uncertainty in acceptor orbital energy, to potential two-state reactivity, and to the influence of the solvent. The correlation trend-lines included here can hence be used as a powerful tool for the rational design of iron−oxo catalysts for C−H activation. The barrier prediction error lies in the 4−11 kJ·mol^{-1} range, an accuracy that is attained by the robustness of the correlation and the wide range of the data set. The approach described has a twofold advantage, assisting the ligand design process in the lab and allowing for very fast screening of potential candidate models that are commercially available. In addition, it links the reactivity with simple molecular orbital concepts that can be applied at no cost for the generation of potential ligand candidates.

Molecular orbital descriptors hence appear to be more than a qualitative analysis tools but they can be transformed in quantitative relations providing key insights for the rational exploration of potentially efficient ligands and catalysts.

METHODS

All calculations were performed using the Gaussian 09 program.[55] Unless stated otherwise, they were performed in the gas-phase and refer to zero Kelvin temperature and ideal gas conditions, which may be different from room temperature experiments in a solution. The DFT functional employed is the OPBE, comprised by the Handy's OPTX modification of Becke's exchange functional (O)[56] and the 1996 correlation functional of Perdew, Burke, and Ernzerhof (PBE).[57] For an additional DFT functional, see the SI Figure S4. Dunning's correlation consistent basis sets where utilized as follows: for the Fe, Cl atoms, the triple-ζ (cc-pVTZ) was employed, while for the C, H, N, and O atoms this was the double-ζ cc-pVDZ.[58] Transition state optimizations were performed using the Berny algorithm[59] and resulted in a structure with a single imaginary frequency that corresponded to the expected methane C−H bond stretch and was followed by intrinsic reaction coordinate calculations (IRC[60]) to verify the link to the expected reactants and products. For many complexes (such as **8**, **15**, and **22**), it was possible to locate both the HS-σ and HS-π path transition states, while for others the σ^*−π^* energy gap was large enough to be prohibitive for locating the energetically disfavored π-path. All barrier values reported are calculated with respect to the "reactant complex" on the same spin surface as the relevant transition state. When a "low spin, LS" complex is mentioned in the text, this indicates a state lying on the triplet/quartet surface, while "high spin, HS" in the quintet/sextet, as per usual. The solvation method utilized is the PCM method as implemented in Gaussian 09.[61−63] It should also be stressed that the work presented here only focuses on the Fe^{IV}=O unstable intermediates of the catalytic cycle. The reported spin gaps (SI Tables S1−S3) should not be confused with, and

DOI: 10.1021/cs500996k
ACS Catal. 2015, 5, 2490−2499

might radically differ, from their respective Fe^{II}/Fe^{III} bare site spin gaps that are reported experimentally.

■ ASSOCIATED CONTENT

Supporting Information

The following file is available free of charge on the ACS Publications website at DOI: 10.1021/cs500996k.

Geometric and energy data, additional correlation plots and counterion effects, Cartesian coordinates of optimized structures, and spin densities (PDF)

■ AUTHOR INFORMATION

Corresponding Author

*E-mail: philippe.sautet@ens-lyon.fr.

Notes

The authors declare no competing financial interest.

■ ACKNOWLEDGMENTS

P.C.A. acknowledges Solvay for the financial support. We also thank the PSMN at ENS de Lyon for computational resources.

■ REFERENCES

(1) Solomon, E. I.; Brunold, T. C.; Davis, M. I.; Kemsley, J. N.; Lee, S.-K.; Lehnert, N.; Neese, F.; Skulan, A. J.; Yang, Y.-S.; Zhou, J. *Chem. Rev.* **2000**, *100* (1), 235−350.

(2) Borovik, A. S. *Chem. Soc. Rev.* **2011**, *40*, 1870−1874.

(3) Costas, M. *Coord. Chem. Rev.* **2011**, *255*, 2912−2932.

(4) Talsi, E. P.; Bryliakov, K. P. *Coord. Chem. Rev.* **2012**, *256*, 1418−1434.

(5) McDonald, A. R.; Que, L., Jr. *Coord. Chem. Rev.* **2013**, *257*, 414−428 and references therein. .

(6) Hohenberger, J.; Ray, K.; Meyer, K. *Nat. Commun.* **2012**, *3*, 720−733.

(7) Rittle, J.; Green, M. T. *Science* **2010**, *330*, 933−937.

(8) Price, J. C.; Barr, E. W.; Tirupati, B.; Bollinger, J. M., Jr.; Krebs, C. *Biochemistry* **2003**, *42*, 7497−7508.

(9) Groves, J. T. *J. Inorg. Biochem.* **2006**, *100*, 434−447.

(10) Cho, K.; Leeladee, P.; McGown, A. J.; DeBeer, S.; Goldberg, D. P. *J. Am. Chem. Soc.* **2012**, *134*, 7392−7399.

(11) Yosca, T.; Rittle, J.; Krest, C. M.; Onderko, E. L.; Silakov, A.; Calixto, J. C.; Behan, R. K.; Green, M. T. *Science* **2013**, *342*, 825−829.

(12) de Visser, S. P. *J. Am. Chem. Soc.* **2010**, *132*, 1087−1097.

(13) Saouma, C. T.; Mayer, J. M. *Chem. Sci.* **2014**, *5*, 21−31.

(14) Evans, M. G.; Polanyi, M. *Trans. Faraday Soc.* **1938**, *34*, 11−24.

(15) Fukui, K.; Yonezawa, T.; Shingu, H. *J. Chem. Phys.* **1952**, *20*, 722−725.

(16) Woodward, R. B.; Hoffmann, R. *Angew. Chem., Int. Ed. Engl.* **1969**, *8*, 781−853.

(17) Mayer, J. M. *Acc. Chem. Res.* **2011**, *44*, 36−46.

(18) Usharani, D.; Janardanan, D.; Li, C.; Shaik, S. *Acc. Chem. Res.* **2013**, *46*, 471−482.

(19) Buda, F.; Ensing, B.; Gribnau, M. C. M.; Baerends, E. J. *Chem. - Eur. J.* **2001**, *7*, 2775−2783.

(20) Buda, F.; Ensing, B.; Gribnau, M. C. M.; Baerends, E. J. *Chem. - Eur. J.* **2003**, *9*, 3436−3444.

(21) Louwerse, M. J.; Baerends, E. J. *Phys. Chem. Chem. Phys.* **2007**, *9*, 156−166.

(22) Decker, A.; Clay, M. D.; Solomon, E. I. *J. Inorg. Biochem.* **2007**, *100*, 697−706.

(23) Ye, S.; Neese, F. *Proc. Natl. Acad. Sci. U. S. A.* **2011**, *108*, 1228−1233.

(24) Decker, A.; Rohde, J.-U.; Klinker, E. J.; Wong, S. D.; Que, L., Jr.; Solomon, E. I. *J. Am. Chem. Soc.* **2007**, *129*, 15983−15996.

(25) Srnec, M.; Wong, S. D.; England, J.; Que, L., Jr.; Solomon, E. I. *Proc. Natl. Acad. Sci. U. S. A.* **2012**, *109*, 14326−14331.

(26) Shaik, S.; Chen, H.; Janardanan, D. *Nat. Chem.* **2011**, *3*, 19−27.

(27) Michel, C.; Baerends, E. J. *Inorg. Chem.* **2009**, *48*, 3628−3638.

(28) Ye, S.; Geng, C.-Y.; Shaik, S.; Neese, F. *Phys. Chem. Chem. Phys.* **2013**, *15*, 8017−830.

(29) Srnec, M.; Dong, S. D.; Solomon, E. I. *Dalton Trans.* **2014**, *43*, 17567−17577.

(30) Britovsek, G. J. P.; England, J.; White, A. J. P. *Inorg. Chem.* **2005**, *44*, 8125−8134.

(31) England, J.; Martinho, M.; Farquhar, E. R.; Frisch, J. R.; Bominaar, E. L.; Münck, E.; Que, L., Jr. *Angew. Chem., Int. Ed.* **2009**, *48*, 3622−3626.

(32) Schröder, D.; Shaik, S.; Schwarz, H. *Acc. Chem. Res.* **2000**, *33*, 139−145.

(33) Bernasconi, L.; Baerends, E. J. *Eur. J. Inorg. Chem.* **2008**, *10*, 1672−1681.

(34) Rohde, J.-U.; In, J.; Lim, M. H.; Brennessel, W. W.; Bukowski, M. R.; Stubna, A.; Münck, E.; Nam, W.; Que, L., Jr. *Science* **2003**, *299*, 1037−1039.

(35) Hong, S.; So, H.; Yoon, H.; Cho, K.-B.; Lee, Y.-M.; Fukuzumi, S.; Nam, W. *Dalton Trans.* **2013**, *42*, 7842−7845.

(36) Wang, D.; Ray, K.; Collins, M. J.; Farquhar, E. R.; Frisch, J. R.; Gomez, L.; Jackson, T. A.; Kerscher, M.; Waleska, A.; Comba, P.; Costas, M.; Que, L., Jr. *Chem. Sci.* **2013**, *4*, 282−291.

(37) England, J.; Guo, Y.; Van Heuvelen, K. M.; Cranswick, M. A.; Rohde, G. T.; Bominaar, E. L.; Münck, E.; Que, L., Jr. *J. Am. Chem. Soc.* **2011**, *133*, 11880−11883.

(38) Seo, M. S.; Kim, N. H.; Cho, K.-B.; So, J. E.; Park, S. K.; Clémancey, M.; Garcia-Serres, R.; Latour, J.-M.; Shaik, S.; Nam, W. *Chem. Sci.* **2011**, *2*, 1039−1045.

(39) Chen, H.; Lai, W.; Shaik, S. *J. Phys. Chem. Lett.* **2010**, *1*, 1533−1540.

(40) Bigi, J. P.; Harman, W. H.; Lassalle-Kaiser, B.; Robles, D. M.; Stich, T. A.; Yano, J.; Britt, R. D.; Chang, C. J. *J. Am. Chem. Soc.* **2012**, *134*, 1536−1542.

(41) Lacy, D. C.; Gupta, R.; Stone, K. L.; Greaves, J.; Ziller, J. W.; Hendrich, M. P.; Borovik, A. S. *J. Am. Chem. Soc.* **2010**, *132*, 12188−12190.

(42) Guell, M.; Luis, J. M.; Sola, M.; Swart, M. *J. Phys. Chem. A* **2008**, *112*, 6384−6391.

(43) Janardanan, D.; Usharani, D.; Chen, H.; Shaik, S. *J. Phys. Chem. Lett.* **2011**, *2*, 2610−2617.

(44) Bernasconi, L.; Louwerse, M. J.; Baerends, E. J. *Eur. J. Inorg. Chem.* **2007**, *19*, 3023−3033.

(45) de Visser, S. P.; Rohde, J.-U.; Lee, Y.-M.; Choc, J.; Nam, W. *Coord. Chem. Rev.* **2013**, *257*, 381−393.

(46) Hong, S.; Hee, S.; Yoon, H.; Cho, K.-B.; Lee, Y.-M.; Fukuzumi, S.; Nam, W. *Dalton Trans.* **2013**, *42*, 7842−7845.

(47) Wang, D.; Ray, K.; Collins, M. J.; Farquhar, E. R.; Frisch, J. R.; Gomez, L.; Jackson, T. A.; Kerscher, M.; Waleska, A.; Comba, P.; Costas, M.; Que, L., Jr. *Chem. Sci.* **2013**, *4*, 282−291.

(48) Sahu, S.; Widger, L. R.; Quesne, M. G.; de Visser, S. P.; Matsumura, H.; Moenne-Loccoz, P.; Siegler, M. A.; Goldberg, D. P. *J. Am. Chem. Soc.* **2013**, *135*, 10590−10593.

(49) Takahashi, A.; Yamaki, D.; Ikemura, K.; Kurahashi, T.; Ogura, T.; Hada, M.; Fujii, H. *Inorg. Chem.* **2012**, *51*, 7296−7305.

(50) Groves, J. T.; Nemo, T. E.; Myers, R. S. *J. Am. Chem. Soc.* **1979**, *101*, 1032−1033.

(51) Khavasi, H. R.; Davarani, S. S. H.; Safari, N. *J. Mol. Catal. A: Chem.* **2002**, *188*, 115−122.

(52) Iamamoto, Y.; Assis, M. D.; Ciuffi, K. J.; Sacco, H. C.; Iwamoto, L.; Melo, A. J. B.; Nascimento, O. R.; Prado, C. M. C. *J. Mol. Catal. A: Chem.* **1996**, *109*, 189−200.

(53) Kang, Y.; Chen, H.; Jeong, Y. J.; Lai, W.; Bae, E. H.; Shaik, S.; Nam, W. *Chem. - Eur. J.* **2009**, *15*, 10039−10046.

(54) Cho, K.; Kim, E. J.; Seo, M. S.; Shaik, S.; Nam, W. *Chem. - Eur. J.* **2012**, *18*, 10444−10453.

(55) Frisch, M. J. *Gaussian 09*, Revision A.02; Gaussian, Inc., Wallingford CT, 2009; full citation in the SI.

(56) Hoe, W. M.; Cohen, A.; Handy, N. C. *Chem. Phys. Lett.* **2001**, *341*, 319−328.

DOI: 10.1021/cs500996k
ACS Catal. 2015, 5, 2490−2499

(57) Perdew, J. P.; Burke, K.; Ernzerhof, M. *Phys. Rev. Lett.* **1996**, *77*, 3865−3868.
(58) Dunning, T. H., Jr. *J. Chem. Phys.* **1989**, *90*, 1007−1023.
(59) Schlegel, H. B. *J. Comput. Chem.* **1982**, *3*, 214−218.
(60) Hratchian, H. P.; Schlegel, H. B. *J. Chem. Theory Comput.* **2005**, *1*, 61−69.
(61) Scalmani, G.; Frisch, M. J. *J. Chem. Phys.* **2010**, *132*, 114110−15.
(62) Improta, R.; Barone, V.; Scalmani, G.; Frisch, M. J. *J. Chem. Phys.* **2006**, *125*, 054103−9.
(63) Improta, R.; Scalmani, G.; Frisch, M. J.; Barone, V. *J. Chem. Phys.* **2007**, *127*, 074504−9.

DOI: 10.1021/cs500996k
ACS Catal. 2015, 5, 2490−2499